Infection dynamics of *Trypanosoma cruzi* in cardiac and skeletal myotubes

José María Eloy Contreras-Ortiz[1,2], Daniel Hernández Mendoza[1,2], Rebeca Manning Cela*[2], Moisés Santillán Zerón*[1]

[1]Centro de Investigación y de Estudios Avanzados del IPN, Unidad Monterrey, Apodaca, NL, México. [2]Departamento de Biomedicina Molecular, Centro de Investigación y de Estudios Avanzados del IPN, CDMX, Ciudad de México, México.
*Email: msantillan@cinvestav.mx; rmanning@cinvestav.mx

SUMMARY

In chronic Chagas' disease, the main organs affected are heart, esophagus, and colon. Despite progress in the understanding of the infection process of its causative agent, *T. cruzi*, little is known about the infectivity and motility of this parasite in cardiomyocytes and skeletal muscle. In this work, we evaluated the dynamics of infection and the motility of *T. cruzi* tripomastigotes, in skeletal myotubes (SM) and cardiac myotubes (CM) differentiated from myoblasts H9c2(2-1) (control), with 1% fetal bovine serum (FBS) and 1% FBS plus retinoic acid, respectively. We determined the invasion efficiency (IE) of the parasite, as well as its infection kinetics (IK), average mean speed (AMS), and mean squared displacement (ʎ), in undifferentiated and differentiated cells. The results showed that SM and CM exhibited a morphological elongation, multiple nuclei, and the expression of TNNI3, indicative of their differentiation. Although the IE and the number of parasites released was the same in undifferentiated and differentiated cells (0.3-0.6%), the CM showed a significant increase in the percentage of infected cells (13.26%) at late stage of IK, compared with SM (3.12%) and MB (3.70 %). A cellular automata model indicates that in CM the free parasite infection propensity was 4×10^{-10}, while the intracellular parasite propensity was 2.15×10^{-2} at the end of the simulation, to obtain the best fitting simulation curves to the experimental data. The parasites decreased their speed (7.95 µm/s) and showed a subdifusive movement (ʎ=0.97) in the presence of undifferentiated and differentiated cells compared to parasites alone (AMS=12.12 µm/s; ʎ=1.006). These results shown that CM are more susceptible to *T. cruzi* infection possibly by a cell-to-cell mechanism of infection, being able to detect the presence of MB, EM, and CM and changing their motility patterns in an independent manner of their differentiation.

KEYWORDS

Cardiac myotube, H9c2(2-1) cells, *Trypanosoma cruzi*, Chagas disease, infection dynamics, average speed, medium quadratic displacement.

INTRODUCTION

Trypanosoma cruzi is a protozoan parasite of medical and biological importance, that is responsible of Chagas disease or American trypanosomiasis, a highly disabling and life-threatening condition that is endemic of tropical areas of Latin America. The disease has been globalized by the migration of infected people from endemic to non-endemic areas, with around 7 million people infected worldwide, an average of 12,000 deaths per year and about 75 million people at risk of infection (WHO, 2022). During disease progression, the most

important conditions are the chronic Chagas cardiomyopathy and digestive megasyndromes that develop during the symptomatic chronic phase (Rassi et al., 2012), where the functionality of the myenteric and cardiac nerve plexus is compromised. Apparently, this is caused by multiple factors such as the host's immune response (Dhiman et al., 2013), the infective and replicating capacity of the parasite, and the motility of *T. cruzi* that has been suggested participates in the success of the infection (Finkelsztein et al., 2015; Arias-del-Angel et al., 2020a; b). Together, this can eventually lead to cardiac and/or digestive failure, leading to the death of the host (Zacks et al., 2005). The parasite has a complex life cycle in which four developmental stages alternate among the insect vector (epimastigote and metacyclic trypomastigote), and the mammalian host (amastigote and blood trypomastigote) where its infective intracellular cycle develops. The trypomastigote, responsible for initiating the infection process in mammals, has a high motility due to its flagellum, which allows its proximity with the membrane of the target cell (Finkelsztein et al., 2015; Arias-del-Angel et al., 2020a). It has been reported that *T. cruzi* can invade a wide variety of non-phagocytic cells in vitro (Andrade and Andrews, 2005; Arias-del-Angel et al., 2020a). This has allowed the study of the infection process of *T. cruzi* in several cell lines related to the cells that become infected at the beginning of the infection when the parasite enters the organism, or those present in organs where the pathology of the disease is established. Examples of this are 3T3 NIH and 3T3-S fibroblasts, Caco2 human colon epithelial cells and H9c2(2-1) myoblast, in which in a previous work, we reported that these cells have different susceptibility to infection by *T. cruzi* (Arias-del-Angel et al., 2020a). In these cells we also studied the dynamics of infection and motility of *T. cruzi*, observing that trypomastigotes change their motility patterns in a specific cell manner, which correlates with their invasion efficiency (Arias-del-Angel et al., 2020a). Based on the parasite's infection kinetics in these four cell lines, we developed a mathematical model that simulates the experimental results, showing that the rate of cell division apparently influences the parasite's invasion efficiency and suggest a possible cell-to-cell mechanism of infection (Arias-del-Angel et al., 2020b). Although cell confluence did not show an important role in the average mean speed of trypomastigotes in 3T3S fibroblasts, NIH 3T3 fibroblasts and Caco2 cells, the parasites decreased their speed in the presence of H9c2(2-1) (2-1) myoblasts to a high confluence, suggesting that it was possibly the result of their differentiation (Arias-del-Angel et al., 2020a). Studies in cell models that are similar to cells that are present in the affected organs during natural infection, are scarce. For example, some studies have evaluated the infection process of *T. cruzi* in cultures of cardiomyocytes obtained from embryonic and neonatal mice, as well as in differentiated cardiomyocytes from human pluripotent cells (Pereira et al., 2017). However, its use is very limited since the cardiomyocytes in culture are highly fragile and have a very short viability in culture (Branco et al., 2015), which makes it difficult to carry out long-term studies as those necessary to understand the infection process of *T. cruzi*.

H9c2(2-1) (2-1) rat ventricular myoblast cells (Hescheler et al., 1991) are precursor cells that can be differentiated in vitro to skeletal myotubes when exposed to a low percentage (1%) of bovine fetal serum (SFB) in the culture medium, or to cardiac myotubes when in addition to growing them with 1% SFB is added retinoic acid to the medium (Ménard et al., 1999; Michailowsky et al., 2001; Branco et al., 2011, 2015; Kankeu et al., 2018). These differentiated cells are characterized by having an elongated form with a parallel arrangement

and partially presenting multinucleated cells (Sardão et al., 2007; Pereira et al., 2011; Kankeu et al., 2018). At the biochemical level, skeletal and cardiac muscle cells have been found to be similar (Branco et al., 2015) and have been reported to express specific isoforms of the L-type calcium channel (Ménard et al., 1999), calsequestrin and troponin I (Kasneci et al., 2009; Branco et al., 2015). The dynamics of infection and the motility of the parasite have not been described in cultures of skeletal and cardiac myotubes obtained by the in vitro differentiation of myoblasts H9c2(2-1) , that could be a biological model like to the skeletal muscle and cardiomyocytes, respectively. Therefore, in the present study we evaluated the dynamics of infection and motility of *T. cruzi* in cells differentiated to skeletal and cardiac myotubes, comparing with the H9c2(2-1) (2-1) myoblasts used as control. We determined the invasion efficiency and kinetics of *T. cruzi* infection and quantified the number of intracellular and released parasites. In addition, we analyzed the motile patterns of the trypomastigotes in the presence of undifferentiated and differentiated cells, determining their average mean speed and mean squared displacement from their trajectories.

MATERIALS AND METHODS

Cell cultures

The 3T3 NIH embryonic mouse fibroblasts (ATCC^{R} CRL-1658^{TM}), and H9c2(2-1) (2-1) rat myoblasts (ATCC^{R} CRL-1446^{TM}) were grown in DMEM (Dulbecco's Modified Eagle Medium [Gibco, ThermoFisher Scientific, USA]), supplemented with 10% fetal bovine serum (FBS) [Gibco, ThermoFisher Scientific, USA], 1% penicillin (10000 u/ml) /streptomycin (10000 µg/ml) [Gibco, ThermoFisher Scientific, USA] at 37° C and 5% CO2. H9c2(2-1) (2-1) myoblasts were cultured when their confluence reached 70% to avoid loss in their differentiation capacity, as this detonates at high confluence (Branco et al., 2015; Arias-del-Angel et al., 2020a).

Parasite culture

Epimastigotes of the CL Brener strain of *T. cruzi* transfected with the vector pTRex-n-GFP (Arias-del-Angel et al., 2020a), were grown in LIT medium (Liver Infusion Tryptose) (Camargo, 1964) supplemented with 10% SFB, 1% penicillin (10000 u/ml)/streptomycin (10000 µg/ml) and hemine at 1% (5 mg/ml) to 28 ° C. For the obtaining of trypomastigotes, we follow the previously published protocol (Manning-Cela et al., 2001; Hernández-Osorio et al., 2010) as briefly described below. A monolayer of NIH 3T3 cells with a confluence of 60-70% was infected with $2x10^{6}$ mid-log-phase epimastigotes in DMEM 2% SFB for 48 h. After this time the parasites were removed by washing the monolayer. The infected cells were maintained in DMEM with 2% SFB, at 37° C and 5% CO2. Only the tripomastigotes released between days 7 and 12 were used for subsequent experiments.

Differentiation of H9c2(2-1) (2-1) cells into skeletal and cardiac myotubes

The H9c2(2-1) (2-1) myoblasts at 60-70 % of confluence were trypsinized, collected, centrifuged at 2100 rpm, and suspended in DMEM with 10 % SFB. Total cells were estimated in a hematocytometer and seeded on glass coverslips of 12 mm diameter in 24-well plate at 600 cells/cm2 for H9c2(2-1) (2-1) myoblasts or 6000 cells/cm2 for skeletal and cardiac myotubes. The plates were incubated 24 hours at 37° C and 5 % CO2 to allow cellular

adhesion. Subsequently the culture medium was replaced as follows: for skeletal and cardiac myotubes, 1 % SFB DMEM was used. In the case of cardiac myotubes was also added daily 1 µM of retinoic acid (AR) [Sigma Aldrich, USA] prepared in dimethylsulfoxide (DMSO) [Sigma Aldrich, USA] (Ménard et al., 1999) for 7 days in darkness (Branco et al., 2015). The H9c2(2-1) (2-1) myoblasts were maintained in DMEM at 10 % SFB. Every third day the culture medium was change and a visual inspection was performed daily to folow the morphological changes in the skeletal and cardiac myotubes. After seven days of differentiation, coverslips were recovered, and the samples fixed with 3.7% formaldehyde for 20 min, permeabilized with acetone at -20° C and stained the actin with rhodamine-phalloidin (Thermo Fisher Scientific, USA) at a dilution of 1:1000, and nuclei with DAPI (Sigma Aldrich, USA) at a dilution of 1:20000. The coverslips were mounted on slides with Vectashield (Vector Laboratories Inc. USA) for analysis. The length and area of the cells, as well as the number of nuclei, were determined using a Leica confocal fluorescence microscope with a 40x objective, and LAS X 3.7.4 2020 (Leica Microsystems CMS GmbH) and the Image J program.

Troponin I3 (TNNI3) detection in H9c2(2-1)

The presence of TNNI3 protein in H9c2(2-1) (2-1) myoblasts and skeletal and cardiac myotubes was determined by Western Blot. Briefly, the H9c2(2-1) (2-1) myoblasts were seeded in 60 mm petri dishes as described above for they differentiation to skeletal and cardiac myotubes. After seven days of differentiation, the cells were collected using trypsin-EDTA (0.05%) and washed twice with 1X PBS (NaCl 0.1 M; K2HPO4 0.01M; KH2PO4 3 mM) by centrifugation at 2100 rpm. The cells were suspended with 250 µl of 1X PBS containing the protease inhibitors PMSF (1mM) [Sigma Aldrich, USA] and 1X Complete (Roche GmbH, DEU). Subsequently, the cells were lysed by three cycles of frozen in liquid N_2 and thawed at 37 ° C. The protein concentration was determined using the Bradford reagent and a standard curve of bovine serum albumin (BSA) at 1mg/ml (Bradford, 1976) as standard, in a 96-well plate reading at 595 nm (Contreras-Ortiz et al., 2017). An aliquot with 25 µg of protein from each extract was mixed with Laemmli 5x buffer (Tris-Cl 60 mM pH 6.8, 2 % SDS, 10 % glycerol, 5 % β-mercaptoethanol, 0.01 % bromophenol blue) and then denatured by boiling for 6 min. Protein extracts were separated by electrophoresis into 12% polyacrylamide gels at 100 volts and 400 mA for 2 hours, and transferred to a nitrocellulose membrane (Bio Rad, USA) in a Mini Trans-Blot (Bio Rad, USA) at 100 volts, 400 mA per hour. To verify the efficiency of protein transfer, the membranes were stained with Ponceau / 1% acetic acid. The membranes were blocked with 6% svelty milk powder in 1X PBS at 4°C overnight and then incubated with a rabbit anti-troponin I3 primary polyclonal antibody (1:500) [Abcam plc, USA] (Branco et al., 2015) in svelty milk at 6% in 1X PBS for 2 hours in agitation. Membranes were washed three times alternately with 1X PBS and 1X/Tween 20 (0.05%) PBS and then incubated with a mouse anti-rabbit IgG-HRP secondary antibody [1:1000] (Santa Cruz Biotechnology Inc. USA) for 1 hour. The membranes were washed again and revealed with the Pierce ECL detection reagent (Thermo Fisher Scientific, USA), recording the signal in a ChemiDoc (BioRad, USA). The mouse anti-GAPDH IgG1κ monoclonal antibody (1:1000) and its secondary goat anti-Mouse IgG (H+L) Cross-Adsorbed, HRP (1:3000) (Invitrogen G-21040), were used as a load control.

Invasion efficiency and kinetics of *T. cruzi* infection, and quantification of the number of intracellular and released parasites.

The H9c2(2-1) (2-1) myoblasts were seeded and differentiated over 12 mm round coverslip in 24-well plate to obtain skeletal and cardiac myotubes, as described above. The cells were infected with 1.8 $x10^5$ tripomastigotes of the CLBr-GFP strain of *T. cruzi* (3 parasites per cell) and allowed the cell-parasite interaction for two hours in DMEM with 2% FBS. The non-adherent parasites were removed washing the monolayers with DMEM medium. The skeletal and cardiac myotubes were incubated with DMEM 2% SFB and the H9c2(2-1) (2-1) myoblasts with DMEM 10 % SFB at 37° C and 5 % CO2. After 18 hours, the coverslips were recovered, fixed, permeabilized, stained, mounted, and analyzed according to the procedure described above. Infected cells were counted in random fields and the invasion efficiency and infection kinetic determined considering the number of infected cells per field multiplied by 100 and divided by the total of cells per field (Arias-del-Angel et al., 2020a). Also, the invasion efficiency was determined after 14 days of differentiation (considering 7 days of differentiation plus 7 days post-infection), following the same experimental strategy. The number of intracellular parasites and the number of parasites released to the supernatant was determined in a Neubauer chamber every day during the infection kinetics.

T. cruzi motility assays

Undifferentiated (The H9c2(2-1) (2-1) myoblasts) and differentiated (skeletal and cardiac myotubes) cells were cultured in 60 mm petri dishes at $3x10^5$ of density, for 12 hours at 37 °C and 5% CO_2. After this time the medium was replaced by DMEM 2 % FBS containing $9x10^5$ tripomastigotes, and $2.7x10^6$ of 0.5µm diameter polymer particles (Fluoro-Max green fluorescent polymer micro spheres, Cat.no. G500) used to monitor internal and external flows to discard experiments in which a flux was detected (Arias-del-Angel et al., 2020a). The samples were maintained at 37 °C and 5% CO2 for 1 hour. The videos were recorded in the middle of the petri dishes at 50 frames per second (640x480 pixels) with a CCD camera using an inverted fluorescence microscope Nikon ECLIPSE TE2000-U and a 40X magnification objective, maintaining the temperature between 37-38 °C. The trajectories of trypomastigotes and polymer particles were recovered by means of a custom software implemented in MatLab in a previous work (Arias-del-Angel et al., 2020a). The trajectories were then statistically analyzed by computing the average mean speed (AMS) and the mean squared displacement (λ). The value of λ determines whether the motion is subdiffusive ($\lambda < 1$), diffusive ($\lambda = 1$), or superdiffusive ($\lambda > 1$).

Statistical analysis

The values of all the experimental measurements are reported as the mean value the standard error, with a 95% confidence interval. The variance analysis test (ANOVA) and a post hoc test were used in experiments with statistical significance. For this analysis the GraphPad Prism 8.0 software package was used (GraphPad software Inc., San Diego, California, EE. UU.). Differences were considered significant at $p < 0.05$.

RESULTS

Myoblasts H9c2(2-1) (2-1) differentiate morphologically and molecularly in skeletal- and cardiac-myotubes.

To study the process of *T. cruzi* infection in skeletal- or cardiac-myotubes, as a possible biological model resembling musculoskeletal and cardiomyocyte, we first established the differentiation conditions according to the literature (Ménard et al., 1999; Branco et al., 2011, 2015). For this, H9c2(2-1) (2-1) myoblasts were cultured in a DMEM medium supplemented with 1% FBS for its differentiation to skeletal myotubes, or in the same medium plus 1 µM of retinoic acid for 7 days for its differentiation to cardiac myotubes. As shown in Figure 1, a cell elongation in both skeletal- (panel B and E) and cardiac-myotubes (panel C and F) was observed in comparison to myoblasts H9c2(2-1) (2-1) (panel A and D), which kept its characteristic starry shape. In addition, multinucleated cells were observed in the differentiated cells to skeletal- (panel E) and cardiac-myotubes (panel F), unlike myoblasts H9c2(2-1) (2-1) (panel D) which were mostly observed mononucleates. To determine whether the observed changes were significant, we performed a quantitative analysis of length and area of the cells, as well as the number of mono and multinucleate cells. As shown in Figure 2, a significant difference was observed in the length, area, and percentage of multinucleated cells between H9c2(2-1) (2-1) myoblasts (261.26 µm/18485.9 µm2/1 %), and cells differentiated to skeletal- (412.94 µm/ 24260.4 µm2/20 %) and cardiac-myotubes (421.48 µm/32344.7 µm2/13.34 %). No statistical difference was observed between the length of skeletal- and cardiac-myotubes, but yes in their area. These morphological changes and number of nuclei indicated a successful differentiation in the conditions used.

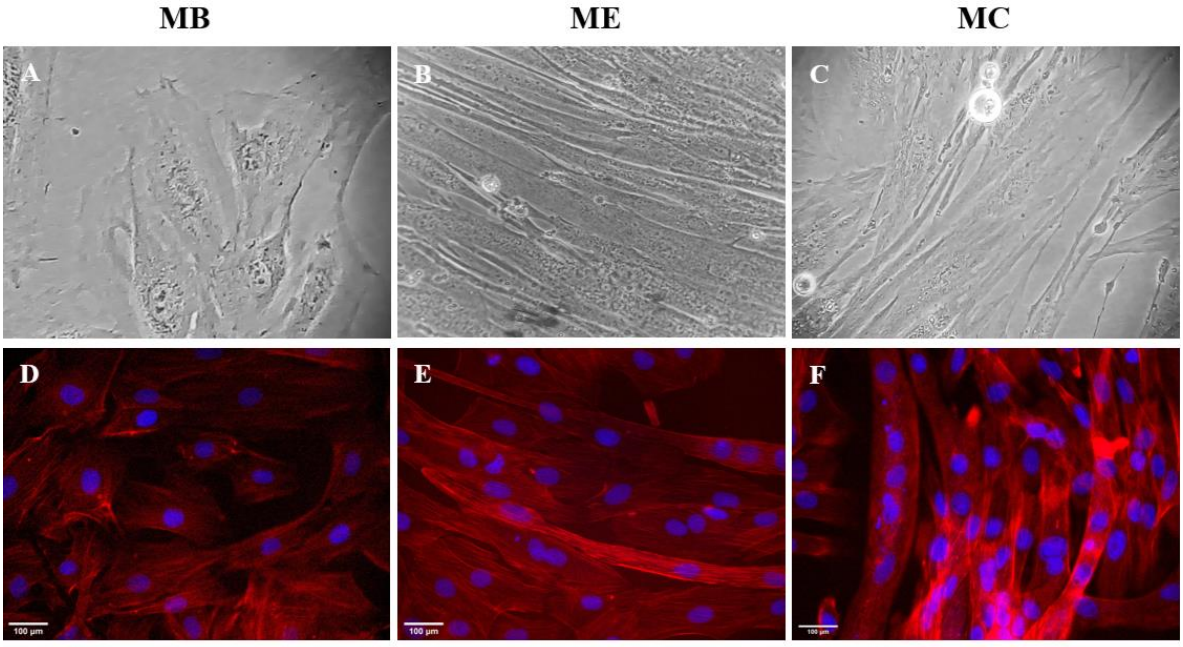

Figure 1. Morphological changes of H9c2(2-1) (2-1) myoblasts differentiated into cardiac- and skeletal-myotubes. H9c2(2-1) (2-1) myoblasts (MB) (control) were differentiated into skeletal myotubes (ME) decreasing the percentage of FBS to 1% in the DMEM medium, or into cardiac myotubes (CM) in DMEM medium 1% FBS plus 1 µM of retinoic acid for 7 days. The cells were analyzed in a phase-contrast inverted microscope with the 20x objective (A, B and C), or in a fluorescence microscope with the 40x objective (D, E and F), after the samples were stained with rhodamine-phalloidin to delimit the actin cytoskeleton (red) and DAPI to dye nuclei.

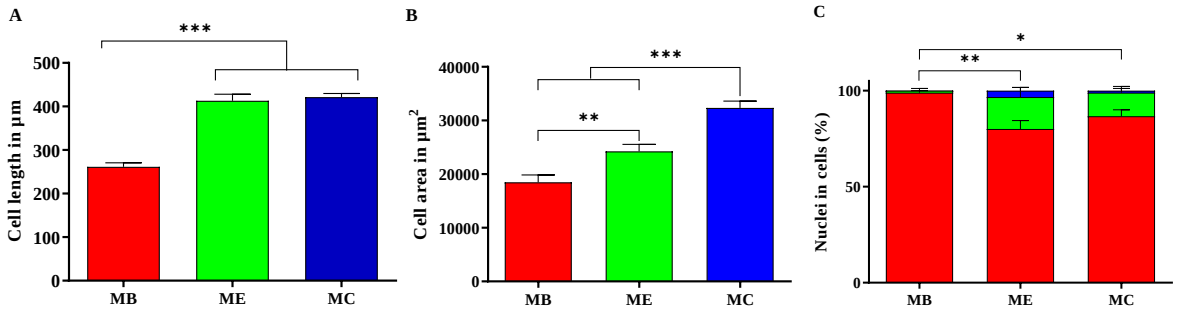

Figure 2. Quantification of morphological changes and number of nuclei of H9c2(2-1) (2-1) myoblasts differentiated to skeletal- and cardiac-myotubes. Length (A), area (B) and percent of mono and multinucleated cells (C) were determined in H9c2(2-1) myoblasts (MB) cultured with 10 % FBS (control) and skeletal myotubes (EM) differentiated in DMEM medium with 1 % SFB, or cardiac myotubes (CM) differentiate in DMEM medium 1 % SFB plus 1 µM of retinoic acid for 7 days. (C) cells with one nucleus (red), two nuclei (green) and three nuclei (blue). The results are the average ± SEM of three independent experiments performed in triplicate each. Statistical comparisons between means were made using an Anova test with the Tukey multiple comparison test (***p<0.001, **p<0.01, *p<0.1 /, *p<0.1 95.00% IQ of difference).

It has been reported that H9c2(2-1) myoblasts when differentiated into skeletal- and cardiac-myotubes express specific proteins (Ménard et al., 1999; Pereira et al., 2011; Branco et al., 2015; Kankeu et al., 2018; Li et al., 2020). Therefore, to corroborate whether the observed morphological transformation was accompanied by the expected molecular changes, we evaluated the presence of troponin I-3 (TNNI3) by the Western Blot technique using specific antibodies, and GAPDH detection as loading control. As seen in Figure 3, a band of approximately 24 kDa was obtained, which is the expected weight for TNNI3, being observed in a smaller proportion in skeletal myotubes, in greater abundance in cardiac myotubes, and absent in H9c2(2-1) myoblasts. These results showed the expected molecular change in the differentiated cells to skeletal- and cardiac-myotubes, thus confirming their successful differentiation.

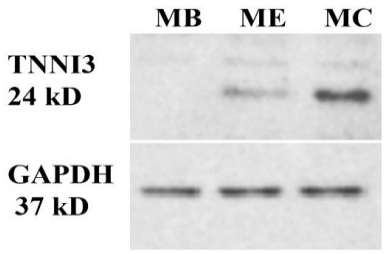

Figure 3. Molecular differentiation of H9c2(2-1) myoblasts to skeletal- or cardiac-myotubes. Total extracts of H9c2(2-1) (MB), skeletal myotubes (EM) and cardiac myoblasts (CM) were obtained and evaluated by Western Blot using a specific antibody against TNNI3, and against to GAPDH as loading control.

T. cruzi invades similarly to H9c2(2-1) (2-1) myoblasts, and skeletal- and cardiac-myotubes.

Once differentiated cells were obtained, we evaluated in them the invasion efficiency of the parasite in comparison to the undifferentiated cells. To do this, the H9c2(2-1) myocytes were differentiated into skeletal- and cardiac-myotubes on coverslips, were infected with the CLBr-GFP tripomastigotes and their invasion efficiency determined. The cells were considered infected when amastigotes were observed inside them being detected from one to three per cell, which is indicative of the fact that tripomastigote was already differentiated into amastigote within the cell and began its multiplication (Figure 4, panel B). No significant statistical differences were observed in the invasion percent of the parasite between H9c2(2-1) myoblasts (0.14%), skeletal myotubes (0.15%) and cardiac myoblasts (0.17%) (Figure 4, panel A), which indicates that the parasite invades differentiated and undifferentiated cells with the same efficiency.

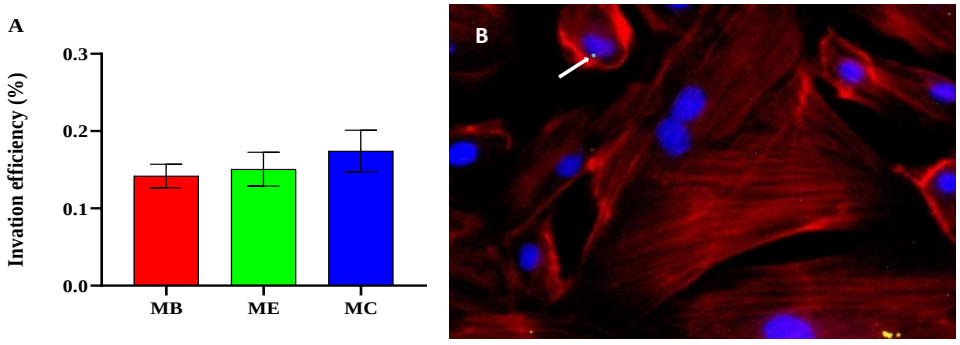

Figure 4. Invasion efficiency of *T. cruzi* in H9c2(2-1) myoblasts, and skeletal- and cardiac-myotubes obtained after seven days of differentiation. A) Percentage of cells infected with *T. cruzi* CLBr-GFP in myoblast H9c2(2-1) (MB), and skeletal- (ME) and cardiac-myotubes (CM), determined at 18 hours post-infection. The results are the average ± SEM of three independent experiments performed in triplicate each. No significant differences were obtained by Anova analysis. B) Micrography of CM cells showing an intracellular GFP-parasite (white arrow), the actin cytoskeleton (red) of the cells stained with rhodamine-phalloidin and the parasite and cells nuclei (blue) stained with DAPI, under the fluorescence microscope.

Cardiac myotubes become more infected with *T. cruzi* than skeletal myotubes and myoblasts H9c2(2-1).

After observing that the parasite invaded similarly the H9c2(2-1) myoblasts, and the skeletal- and cardiac-myotubes, we evaluated the infection kinetics in them. To do this,

undifferentiated and differentiated cells on coverslip were infected with the same amount of CLBr-GFP trypomastigotes for two hours and the percentage of infected cells was determined every 24 hours for 7 days. As shown in Figure 5, in the first 5 days of infection the number of infected cells increased slightly in the same proportion in both undifferentiated and differentiated cells. However, after this time the cardiac myotubes showed a significant increase in the percentage of infected cells at day 7 (13.26%) post-infection, in comparison to the skeletal myotubes (3.15%) and H9c2(2-1) myoblasts (3.70%). Indicating that the cardiac myotubes are more susceptible to infection by the parasite at long times.

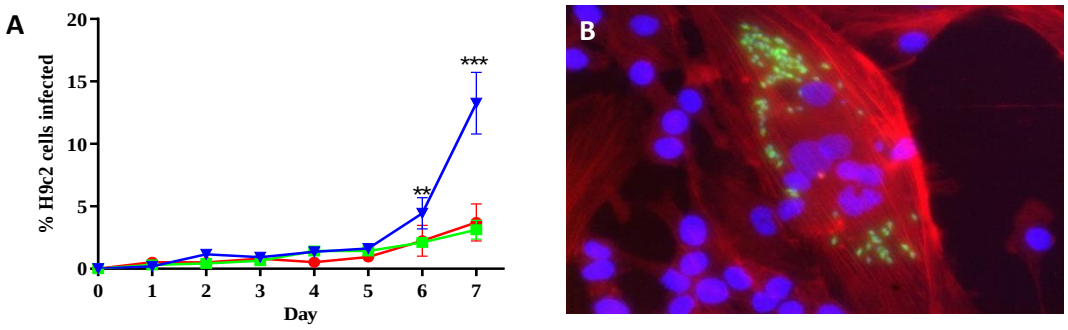

Figure 5. Kinetics of *T. cruzi* infection in H9c2(2-1) myoblasts, and skeletal- and cardiac-myotubes. A) Percent of infected cells of H9c2(2-1) myoblast (red), skeletal myotubes (green), and heart myotubes (blue) infected with *T. cruzi* CLBr-GFP, determined every 24 hours during seven days. The results are the average ±SEM of three independent experiments performed in triplicate each. Statistical comparisons were made between medians using an Anova test with the Tukey multiple comparison test (***p<0.0001, **p<0.01 / 95.00% IQ of difference). B) Fluorescence micrography representative of a multinucleated skeletal myotube (blue) infected with *T. cruzi* CLBr-GFP (green), showing the actin cytoskeleton (red) of the cells stained with rhodamine-phalloidin and the parasite and cells nuclei (blue) stained with DAPI, under the fluorescence microscope.

The number of intracellular parasites in skeletal- and cardiac-myotubes is higher than in H9c2(2-1) myoblasts in late infection, but the number of released parasites to the supernatant is the same, in both the undifferentiated and differentiated cells.

Above it was shown that undifferentiated and differentiated cells have similar invasion efficiencies by *T. cruzi*, but the cardiac myotubes are more infected at days 6 and 7 of the infection kinetic (Figure 4 and 5). One possible explanation for these results is that the greater area observed in the cardiac myotubes (Figure 2) could host a greater number of parasites per infected cell, releasing more parasites to the supernatant and consequently infecting more cells at long times. Therefore, we quantified the number of intracellular parasites (Figure 6) and the number of released parasites to the supernatant (Figure 7) in the undifferentiated and differentiated cells, through the infection kinetics. As shown in Figure 6, in the first five days of infection no difference was observed in the number of intracellular parasites in undifferentiated and differentiated cells. At day six post-infection, a significant increase in intracellular parasites was observed in skeletal myotubes (51 PI on average) but not in cardiac myotubes (43 PI on average), compared with H9c2(2-1) myoblasts (32 PI on average). Finally, at day 7 post-infection the number of intracellular parasites in both skeletal myotubes

(57 PI) and cardiac (66 PI) myotubes was significantly higher than that of H9c2(2-1) myoblasts (37 PI). Despite these differences, when we quantified the released parasites to the supernatant, no significant differences were observed between the three types of cells (Figure 7). This suggests that the observed increase in the percentage of infection in the cardiac myotubes at the sixth- and seventh-day post-infection, is not the result of a greater number of parasites released to the supernatant that could infect secondarily a greater number of cells.

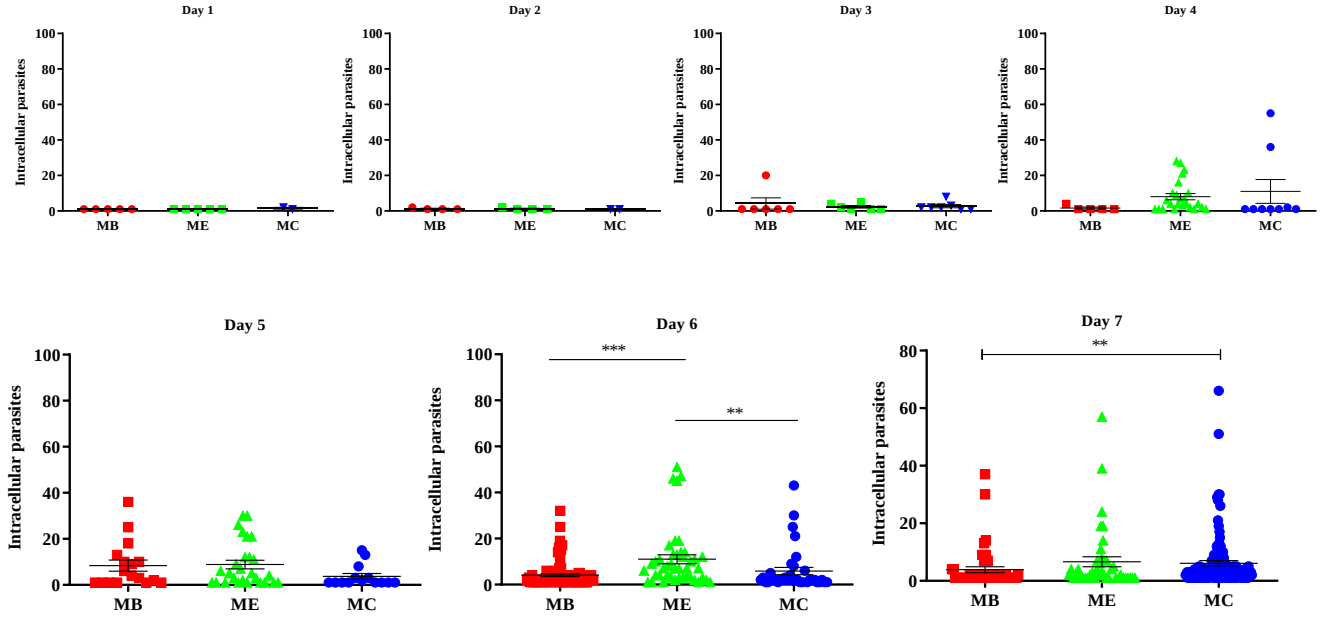

Figure 6. Number of intracellular parasites in H9c2(2-1) myoblasts, and skeletal- and cardiac-myotubes. H9c2(2-1) myoblasts (MB), skeletal myotubes (ME), and cardiac myotubes (CM) were infected with trypomastigotes CLBr-GFP of *T. cruzi* and the number of intracellular parasites quantified every 24 hours through the infection kinetic. The results are the average ± SEM of three independent experiments performed in triplicate each. Statistical comparisons were made between medians using a Kruskal-Wallis's test with the Dunn multiple comparison test (***p<0.0001, **p<0.01, *p<0.1 / 95.00% IQ of difference).

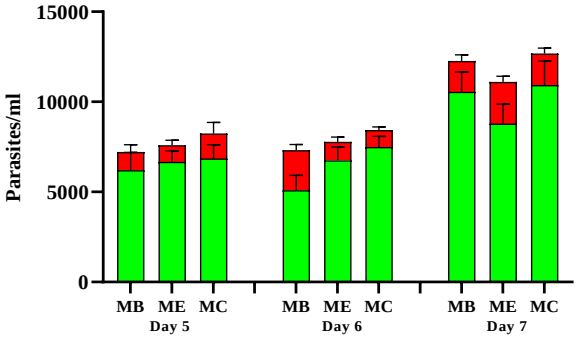

Figure 7. Number of parasites released in the supernatant of H9c2(2-1) myoblasts, and skeletal- and cardiac-myotubes. H9c2(2-1) myoblasts (MB), skeletal myotubes (ME), and cardiac myotubes (MC) were infected with trypomastigotes CLBr-GFP of *T. cruzi*, and the number of parasites released in the supernatant at days 5, 6 and 7 post-infections was determined. The results are the average ± SEM of three independent experiments performed in triplicate each. No significant differences were obtained by Anova analysis.

The invasion efficiency of *T. cruzi* in the cardiac myotubes remains unchanged at prolonged times of differentiation.

Another possibility that could explain the increase of infected cells in the cardiac myotubes at late stages of the kinetics of infection, is that these cells somehow modified their susceptibility to *T. cruzi* invasion at prolonged times of differentiation (seven days of differentiation plus 7 days of infection kinetics). Therefore, we evaluated the invasion efficiency of *T. cruzi* in the cardiac myotubes at day fourteen after their differentiation began and compared it with that obtained in the skeletal myotubes at the same time of differentiation, and H9c2(2-1) myoblasts as control. As shown in Figure 8, no differences in the invasion efficiency were observed between the three types of cells analyzed, which indicates that this parameter is not responsible for the greater number of infected cells observed in the cardiac myotubes at day 6 and 7 post-infection.

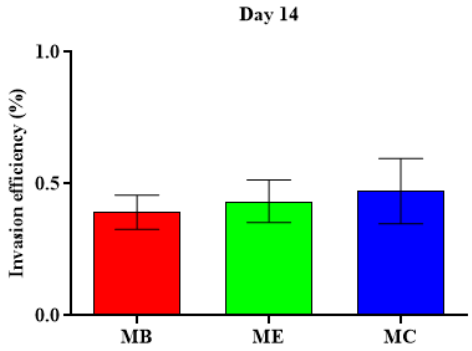

Figure 8. Invasion efficiency of *T. cruzi* in H9c2(2-1) myoblasts, and skeletal- and cardiac-myotubes obtained after fourteen days of differentiation. Percentage of cells infected with *T. cruzi* CLBr-GFP in myoblast H9c2(2-1) (MB), and skeletal- (ME) and cardiac-myotubes (CM) obtained after fourteen days of differentiation, determined at 18 hours post-infection. The results are the average ± SEM of three independent experiments performed in triplicate each. No significant differences were obtained by Anova analysis.

As time progresses of the infection kinetics, cell-to-cell infection apparently is more frequent in cardiac myotubes.

Previously we reported a mathematical model to simulate the experimental outcomes of infection-kinetics of various cell lines (Arias-del-Angel et al., 2020b). It was considered three different version models, of which the most complete model contemplated cell-to-cell infections and replication of infected cells. The results showed that cell-to-cell infections

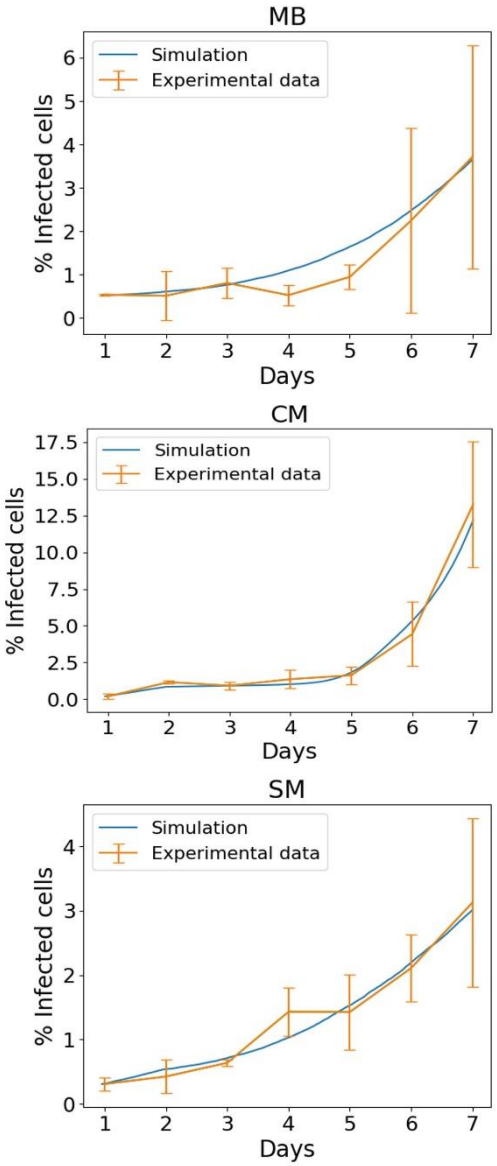

plays an important role during the kinetics of *T. cruzi* infections, while the replication of infected cells is not so important from an infection-dynamics perspective. Therefore, we use a mathematical approach to know if cell-to-cell infection could be participating in the increase in the number of infected cells in cardiac myotubes. A cellular automata model was developed to better understand the dynamics of the infection in the experimental data. Model parameters where optimized to obtain the best fitting simulation curves to the experimental data. Curve fitting was performed by nonlinear least square. Two ways of infection were added to the model, infection of cells by interaction with free parasites in the medium, and infection of cells by contact with infected cells in its neighborhood. The first type of infection depends on the number of free parasites in the medium, while the second type depends on the number of intracellular parasites the cells in the neighborhood harbors. For the MB group, a Moore neighborhood was used, meanwhile a Von Neuman neighborhood was used for the CM and SM groups. The best fitting curves for each group are shown in the Figure 9. For the MB and SM groups, fitting was achieved with a constant set of optimized parameters: 3×10^{-11} and 1×10^{-10} parasites^{-1} h^{-1} for free parasite infection, and 5.25×10^{-4} and 1×10^{-3} intracellular parasites^{-1} h^{-1}, respectively. Most experimental points are close to the simulation curve, except for some points, that can be considered experimental or biological variations, as each experimental point comes from individual cultures. For the CM group, free parasite infection propensity was 4×10^{-10}, but an adjustment of the cell-to-cell infection propensity to a time-depending Hill function was required to achieve the best fitting. Hill equation's optimized parameters n, k and y max were 10, 156 and 0.0215, respectively, with a propensity of 2.15×10^{-2} intracellular parasites^{-1} h^{-1} at the end of the simulation. This suggests that, as time progresses, cell-to-cell infection should be more frequent, since intracellular parasites grow in number with time, and even, that cell-to-cell infection can be activated in some time instant or number of intracellular parasites.

Figure 9. Time evolution of the fraction of infected cells in infection kinetics experiments in H9c2(2-1) myoblasts, and skeletal- and cardiac-myotubes, and infection simulations. Orange lines represent experimental values (averaged over 3 independent experiments), while the error bars denote standard deviations. Blue lines correspond to the best fitting curves

obtained from simulations of the cellular automata model, with the corresponding error bars denoting standard deviations. MB: Myoblasts, CM: Cardio Myotubes, SM: Skeletal Myotubes.

The *T. cruzi* movement is subdifusive and changes in the presence of cells independently of their differentiation.

In a previous study, we reported that trypomastigotes change their motility patterns according to cell type (NIH, 3T3 S, CaCo2 and H9c2(2-1)) and that they decrease their speed in the presence of H9c2(2-1) (2-1) myoblasts at a high confluence, possibly because of their differentiation (Arias-del-Ángel et al., 2020a). Therefore, we evaluated the average speed and the mean quadratic displacement of the tripomastigotes in the presence of undifferentiated cells (H9c2(2-1) myoblasts) and differentiated to skeletal and cardiac myotubes, and we include cell-free parasites and fluorescent polymer microspheres as control. As can be seen in Figure 10, trypomastigotes decreased significantly and at the same magnitude their average speed in the presence of H9c2(2-1) myoblasts (7.74 microns/s), skeletal myotubes (8.43 microns/s) and cardiac myotubes (7.70 microns/s), compared to parasites alone (12.12 microns/s). The measured average particle velocity (PT) [1.44 microns/s] confirmed that there were no external or internal flows that could alter the path of the parasites (panel A). With respect to the mean quadratic displacement (ʎ), indicative of both tripomastigotes moving from an initial position, as in the previous work (Arias-del-Ángel et al., 2020a), it was observed that in the parasites without cells their movement is approximately diffusive (ʎ from 2006). Whereas in parasites in the presence of myoblasts (0.9730), skeletal myotubes (0.9775) and cardiac myotubes (0.9745) the value of ʎ is less than one and therefore its movement is subdifusive, without observing statistical difference between these three cell types (panel B). These results indicate that the motility pattern of *T. cruzi* changes in the presence of cells with a subdifusive movement, tending to stay in more restricted areas, and that this does so independently of cell differentiation.

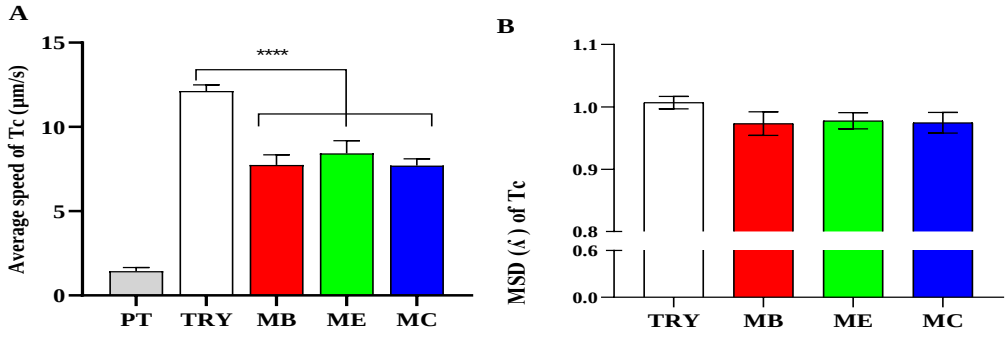

Figure 10. Average speed and mean quadratic displacement (ʎ) of Trypanosoma cruzi in culture of H9c2(2-1) myoblasts, skeletal and cardiac myotubes. Mean velocity (A) and mean quadratic displacement [ʎ] (B) values of *T. cruzi* tripomastigotes determined from parasite trajectories in the presence of H9c2(2-1) (MB) myoblast cultures, skeletal myotubes (ME) and cardiac myotubes (MC). Tripomastigotes alone in culture (TRY) and polymer microspheres (PT) were used as control. The results are the average SEM of three independent experiments performed in triplicate each. Statistical comparisons between means were made using an Anova test with the Tukey multiple comparison test (***p<0.0001 / 95.00% IQ difference).

REFERENCIAS

Alves, L. G. A., Scariot, D. B., Guimarães, R. R., Nakamura, C. V., Mendes, R. S. and Ribeiro, H. V. (2016). Transient superdiffusion and long-range correlations in the motility patterns of trypanosomatid flagellate protozoa. *PLoS ONE* **11**, 1–15. doi: 10.1371/journal.pone.0152092.

Andrade, L. O. and Andrews, N. W. (2005). Opinion: The Trypanosoma cruzi - Host-cell interplay: Location, invasion, retention. *Nature Reviews Microbiology* **3**, 819–823. doi: 10.1038/nrmicro1249.

Arias-del-Angel, J. A., Santana-Solano, J., Santillán, M. and Manning-Cela, R. G. (2020a). Motility patterns of Trypanosoma cruzi trypomastigotes correlate with the efficiency of parasite invasion in vitro. *Scientific Reports* **10**, 1–11. doi: 10.1038/s41598-020-72604-4.

Arias-del-Angel, J. A., Manning-Cela, R. G. and Santillán, M. (2020b). Dynamics of Mammalian Cell Infection by Trypanosoma cruzi trypomastigotes. *Frontiers in Microbiology* **11**, 1–11. doi: 10.3389/fmicb.2020.559660.

Balmer, J. E. and Blomhoff, R. (2002). Gene expression regulation by retinoic acid. *Journal of Lipid Research* **43**, 1773–1808. doi: 10.1194/jlr.R100015-JLR200.

Bedada, F. B., Chan, S. S. K., Metzger, S. K., Zhang, L., Zhang, J., Garry, D. J., Kamp, T. J., Kyba, M. and Metzger, J. M. (2014). Acquisition of a quantitative, stoichiometrically conserved ratiometric marker of maturation status in stem cell-derived cardiac myocytes. *Stem Cell Reports* **3**, 594–605. doi: 10.1016/j.stemcr.2014.07.012.

Bradford, M. M. (1976). A Rapid and Sensitive Method for the Quantitation of Microgram Quantities of Protein Utilizing the Principle of Protein-Dye Binding. *ANALYTICAL BIOCHEMISTRY* **72**, 248–254.

Branco, A. F., Pereira, S. L., Moreira, A. C., Holy, J., Sardão, V. A. and Oliveira, P. J. (2011). Isoproterenol cytotoxicity is dependent on the differentiation state of the cardiomyoblast H9c2(2-1) cell line. *Cardiovascular Toxicology* **11**, 191–203. doi: 10.1007/s12012-011-9111-5.

Branco, A. F., Pereira, S. P., Gonzalez, S., Gusev, O., Rizvanov, A. A. and Oliveira, P. J. (2015). Gene expression profiling of H9c2(2-1) myoblast differentiation towards a cardiac-like phenotype. *PLoS ONE* **10**, 1–18. doi: 10.1371/journal.pone.0129303.

Camargo, E. (1964). Growth and differentiation in Trypanosoma cruzi. I. Origin of metacyclic trypanosomes in liquid media. *Rev Inst Med São Paulo* **6**, 93–100.

Contreras-Ortiz, J. M. E., Barbabosa-Pliego, A., Oros-Pantoja, R., Aparicio-Burgos, J. E., Zepeda-Escobar, J. A., Hassan-Moustafa, W. H., Ochoa-García, L., Uxúa Alonso-Fresan, M., Tenorio Borroto, E. and Vázquez-Chagoyán, J. C. (2017). Effects of astaxanthin in mice acutely infected with *Trypanosoma cruzi*. *Parasite* **24**, 17. doi: 10.1051/parasite/2017018.

Dhiman, M., Coronado, Y. A., Vallejo, C. K., Petersen, J. R., Ejilemele, A., Nu??ez, S., Zago, M. P., Spratt, H. and Garg, N. J. (2013). Innate Immune Responses and Antioxidant/Oxidant Imbalance Are Major Determinants of Human Chagas Disease. *PLoS Neglected Tropical Diseases* **7**,. doi: 10.1371/journal.pntd.0002364.

Ferreira, É. R., Bonfim-Melo, A., Mortara, R. A. and Bahia, D. (2012). Trypanosoma cruzi extracellular amastigotes and host cell signaling: More pieces to the puzzle. *Frontiers in Immunology* **3**, 1–6. doi: 10.3389/fimmu.2012.00363.

Finkelsztein, E. J., Diaz-Soto, J. C., Vargas-Zambrano, J. C., Suesca, E., Guzmán, F., López, M. C., Thomas, M. C., Forero-Shelton, M., Cuellar, A., Puerta, C. J. and

González, J. M. (2015). Altering the motility of Trypanosoma cruzi with rabbit polyclonal anti-peptide antibodies reduces infection to susceptible mammalian cells. *Experimental Parasitology* **150**, 36–43. doi: 10.1016/j.exppara.2015.01.007.

Florencio-Martínez, L., Márquez-Dueñas, C., Ballesteros-Rodea, G., Martínez-Calvillo, S. and Manning-Cela, R. (2010). Cellular analysis of host cell infection by different developmental stages of Trypanosoma cruzi. *Experimental Parasitology* **126**, 332–336. doi: 10.1016/j.exppara.2010.04.015.

Guo, Y. and Pu, W. T. (2020). Cardiomyocyte maturation: New phase in development. *Circulation Research* 1086–1106. doi: 10.1161/CIRCRESAHA.119.315862.

Hescheler, J., Meyer, R., Plant, S., Krautwurst, D., Rosenthal, W. and Schultz, G. (1991). Morphological, biochemical, and electrophysiological characterization of a clonal cell (H9c2(2-1)) line from rat heart. *Circulation Research* **69**, 1476–1486. doi: 10.1161/01.RES.69.6.1476.

Kankeu, C., Clarke, K., Van Haver, D., Gevaert, K., Impens, F., Dittrich, A., Roderick, H. L., Passante, E. and Huber, H. J. (2018). Quantitative proteomics and systems analysis of cultured H9C2(2-1) cardiomyoblasts during differentiation over time supports a "function follows form" model of differentiation. *Molecular Omics* **14**, 181–196. doi: 10.1039/c8mo00036k.

Kasneci, A., Kemeny-Suss, N. M., Komarova, S. V. and Chalifour, L. E. (2009). Egr-1 negatively regulates calsequestrin expression and calcium dynamics in ventricular cells. *Cardiovascular Research* **81**, 695–702. doi: 10.1093/cvr/cvn357.

Ley V., Andrews N. W., Robbins E. S., N. V. (1988). Amastigotes of Trypanosoma cruzi sustain an infective cycle in mammalian cells. *Memórias do Instituto Oswaldo Cruz* **83 Suppl 1**, 452–455. doi: 10.1590/S0074-02761988000500045.

Li, Q., Zhang, T., Zhang, R., Qin, X. and Zhao, J. (2020). All-trans retinoic acid regulates sheep primary myoblast proliferation and differentiation in vitro. *Domestic Animal Endocrinology* **71**,. doi: 10.1016/j.domaniend.2019.106394.

Liu, B., Li, N., Jiang, Y., Liu, C., Ma, L., Cong, W. and Xiao, J. (2016). Effects of excessive retinoic acid on C2C12 myogenesis. *Journal of Hard Tissue Biology* **25**, 97–103. doi: 10.2485/jhtb.25.97.

Maire, A., Teyssier, C., Balaguer, P., Bourguet, W. and Germain, P. (2019). RAR-Specific Ligands and Their Combinations. *Cells* **8**, 1–24.

Manning-Cela, R., Cortés, A., González-rey, E., Voorhis, W. C. Van, Swindle, J. and González, A. (2001). LYT1 protein is required for efficient in vitro infection by Trypanosoma cruzi. *Infection and ...* **69**, 3916–3923. doi: 10.1128/IAI.69.6.3916.

Ménard, C., Pupier, S., Mornet, D., Kitzmann, M., Nargeot, J. and Lory, P. (1999). Modulation of L-type calcium channel expression during retinoic acid- induced differentiation of H9C2(2-1) cardiac cells. *Journal of Biological Chemistry* **274**, 29063–29070. doi: 10.1074/jbc.274.41.29063.

Michailowsky, V., Silva, N. M., Rocha, C. D., Vieira, L. Q., Lannes-Vieira, J. and Gazzinelli, R. T. (2001). Pivotal role of interleukin-12 and interferon-gamma axis in controlling tissue parasitism and inflammation in the heart and central nervous system during Trypanosoma cruzi infection. *The American journal of pathology* **159**, 1723–33. doi: 10.1016/S0002-9440(10)63019-2.

Moreira-Leite, F. F., Sherwin, T., Kohl, L. and Gull, K. (2001). A trypanosome structure involved in transmitting cytoplasmic information during cell division. *Science* **294**, 610–612. doi: 10.1126/science.1063775.

OMS (2022). *La enfermedad de Chagas (tripanosomiasis americana)*.

Pereira, S. L., Ramalho-Santos, J., Branco, A. F., Sardão, V. A., Oliveira, P. J. and Carvalho, R. A. (2011). Metabolic remodeling during H9c2(2-1) myoblast differentiation: Relevance for in vitro toxicity studies. *Cardiovascular Toxicology* **11**, 180–190. doi: 10.1007/s12012-011-9112-4.

Pereira, P. D., Capila, R. F., do Couto, N. F., Estrada, D., Gadelha, F. R., Radi, R., Piacenza, L. and Andrade, L. O. (2017). Cardiomyocyte oxidants production may signal to *T. cruzi* intracellular development. *PLoS Neglected Tropical Diseases* **11**, 1–23. doi: 10.1371/journal.pntd.0005852.

Pereira, S. S., Trindade, S., De Niz, M. and Figueiredo, L. M. (2019). Tissue tropism in parasitic diseases. *Open Biology* **9**,. doi: 10.1098/rsob.190036.

Ranatunga, M., Rai, R., Richardson, S. C. W., Dyer, P., Harbige, L., Deacon, A., Pecorino, L. and Getti, G. T. M. (2020). Leishmania aethiopica cell-to-cell spreading involves caspase-3, AkT, and NF-κB but not PKC-δ activation and involves uptake of LAMP-1-positive bodies containing parasites. *FEBS Journal* **287**, 1777–1797. doi: 10.1111/febs.15166.

Rassi, A., Rassi, A. and Marcondes de Rezende, J. (2012). American Trypanosomiasis (Chagas Disease). *Infectious Disease Clinics of North America* **26**, 275–291. doi: 10.1016/j.idc.2012.03.002.

Real, F., Florentino, P. T. V., Reis, L. C., Ramos-Sanchez, E. M., Veras, P. S. T., Goto, H. and Mortara, R. A. (2014). Cell-to-cell transfer of Leishmania amazonensis amastigotes is mediated by immunomodulatory LAMP-rich parasitophorous extrusions. *Cellular Microbiology* **16**, 1549–1564. doi: 10.1111/cmi.12311.

Saenz-Garcia, J. L., Borges, B. S., Souza-Melo, N., Machado, L. V., Miranda, J. S., Pacheco-Lugo, L. A., Moretti, N. S., Wheleer, R., Soares Medeiros, L. C. and DaRocha, W. D. (2022). Trypanin Disruption Affects the Motility and Infectivity of the Protozoan Trypanosoma cruzi. *Frontiers in Cellular and Infection Microbiology* **11**, 1–17. doi: 10.3389/fcimb.2021.807236.

Sardão, V. A., Oliveira, P. J., Holy, J., Oliveira, C. R. and Wallace, K. B. (2007). Vital imaging of H9c2(2-1) myoblasts exposed to tert-butylhydroperoxide - Characterization of morphological features of cell death. *BMC Cell Biology* **8**, 1–15. doi: 10.1186/1471-2121-8-11.

Sosa-Hernández, E., Ballesteros-Rodea, G., Arias-Del-Angel, J. A., Dévora-Canales, D., Manning-Cela, R. G., Santana-Solano, J. and Santillán, M. (2015). Experimental and mathematical-modeling characterization of Trypanosoma cruzi epimastigote motility. *PLoS ONE* **10**, 1–17. doi: 10.1371/journal.pone.0142478.

Spudich, J. A. and Watt, S. (1971). The Regulation of Rabbit Skeletal Muscle Contraction. *Journal of Biological Chemistry* **246**, 4866–4871. doi: 10.1016/s0021-9258(18)62016-2.

Stefanovic, S. and Zaffran, S. (2017). Mechanisms of retinoic acid signaling during cardiogenesis. *Mechanisms of Development* **143**, 9–19. doi: 10.1016/j.mod.2016.12.002.

Uppaluri, S., Nagler, J., Stellamanns, E., Heddergott, N., Herminghaus, S., Engstler, M. and Pfohl, T. (2011). Impact of microscopic motility on the swimming behavior of parasites: Straighter Trypanosomes are more directional. *PLoS Computational Biology* **7**, 1–8. doi: 10.1371/journal.pcbi.1002058.

Zacks, M., Wen, J. J., Vyatkina, G., Bhatia, V. and Garg, N. (2005). An overview of chagasic cardiomyopathy: Pathogenic importance of oxidative stress. *Anais da Academia Brasileira de Ciencias* **77**, 695–715. doi: 10.1590/S0001-

37652005000400009.